Available online at www.sciencedirect.com

ScienceDirect

Advances in Space Research 71 (2023) 3394–3407

ADVANCES IN SPACE RESEARCH (a COSPAR publication)

www.elsevier.com/locate/asr

Observed (GPS) and modeled (IRI and TIE-GCM) TEC trends over southern low latitude during solar cycle-24

S.S. Rao [a,*], Monti Chakraborty [b], A.K. Singh [c]

[a] Udaipur Solar Observatory/Physical Research Laboratory, Udaipur 313001, India
[b] Departmentof Electronics and Communication Engineering, Tripura University, Agartala 799022, India
[c] Department of Physics, Institute of Science, Banaras Hindu University, Varanasi 221005, India

Received 27 July 2022; received in revised form 30 November 2022; accepted 14 December 2022
Available online 20 December 2022

Abstract

The Total Electron Content (TEC) derived from the Global Positioning System (GPS) measurements during the solar cycle-24 at COCO Island (12.20^0 S, 96.80^0 E) are compared with those of International Reference Ionosphere-2016 (IRI-2016) model and Thermosphere Ionosphere Electrodynamics General Circulation Model (TIE-GCM). TEC data derived from the above two models follow the nature of observed variations with considerable divergences in amplitudes. The precision of model TEC in reference to GPS TEC is discussed using a correlation coefficient, mean difference, root mean square error, and relative deviation module mean techniques. The randomness of predictions is found to be biased by the solar cycle, season, and local time. The simulated values showed better accuracy during the low solar activity and night hours. This study is an extension of Rao et al. (2019b), in which we reported similar study of TEC variability at the northern low latitude station. First of all, it is observed from two studies that the magnitude of TEC is greater at the southern low latitude than at the northern low latitude. Also the correlation between GPS TEC/ IRI TEC and F10.7 flux is determined to be greater at northern low latitude station compared to southern low latitude station. However, TIE-GCM TEC values are found to be slightly more correlated with F10.7 flux at southern low latitude station compared to northern low latitude station. With regard to seasonal variation, semiannual oscillations in TEC are found to be coherent on both sides of the equator. However, the winter anomaly is not observed or predicted by models at the southern low latitude whereas it is observed to be a solar flux-dependent feature at the northern low latitude. The IRI model closely follows seasonal trends of TEC whereas TIE-GCM over-predicted TEC during solstices at the northern low latitudes. Models TEC deviations are found to be lesser at the southern low latitude compared to northern low latitude.

Keywords: GPS; IRI model; TIE-GCM; TEC; Southern Low Latitude

1. Introduction

The low latitude ionosphere shows a distinct feature as compared to the mid and high latitude ionosphere due to the presence of equatorial ionization anomaly (EIA) caused by the fountain effect. The $\mathbf{E} \times \mathbf{B}$ force in the equatorial zone uplifts plasma to greater heights, which disperses along magnetic field lines under the gravitational and pressure gradient forces and finally results in EIA (Martyn 1953; Kendall 1964; Duncan 1969). The EIA is regulated by the equatorial electrojet (EEJ) which is a jet current in the E region developed due to the Sq-current system. The Sq-current system is generated due to the global solar-driven wind flowing across the field lines. As a result, significant variations in the electron density of the low lat-

* Corresponding author.
E-mail addresses: ssraophy116@gmail.com, ssraophy116@gmail.com (S.S. Rao), montichakraborty@tripurauniv.in (M. Chakraborty), singhak@bhu.ac.in (A.K. Singh).

https://doi.org/10.1016/j.asr.2022.12.030
0273-1177/

itude ionosphere are observed with local time, latitude and altitude. (Pacheco and Yizengaw 2013; Chen et al. 2016).

The asymmetry of EIA between the two hemispheres is linked with the inter-hemispheric wind streaming from the north to the south and the difference between magnetic fields. In addition, the spatial and temporal inconstancy of the EUV radiation and thermospheric composition directly influences NmF2. Therefore, notable diurnal, seasonal (semiannual and annual), and solar cycle variations in electron density depending upon different geophysical conditions are observed. The electron density depends on the photoionizing radiation which changes with changing sun-earth distance and neutral compositions (Chapman 1931).

The variations in ionospheric electron density unfollowing Chapman's assumption are referred as anomalies (Rishbeth 1998). For example, the maximum daytime electron concentrations are often found greater in winter and equinoxes than in summer despite the larger quantity of available solar flux due to small solar zenith angle (Rishbeth and Setty 1961; Rishbeth and Mullar-Wodarg 2006). The semiannual variation in the F region ionosphere is a consistent feature observed during all solar cycles at all latitudes (Mayr & Mahajan 1971; Millward et al. 1996). However, strength of semiannual peaks may be different during vernal and autumn and also may depend upon longitude (e.g., Balan et al. 2000; Ma et al. 2003). The seasonal anomaly over the northern low and mid-latitudes is a consistent characteristic in foF2 (Pulido and Francisco 1997; Wang et al. 2017), while in TEC it becomes a solar flux dependent phenomenon (Yasyukevich et al. 2018; Rao et al. 2019a). Annual anomaly is characterised by the greater NmF2 in December than in June on a global scale (Zou et al. 2000). In the December solstice, the Southern Hemisphere receives the maximum intensity of the solar flux due to tilt in the Earth's axis of rotation. This is the reason for the dominating presence of annual anomaly over the southern hemisphere. TEC anomalies are the direct consequence of orbitally driven photoionization and thermospheric compositional variations (Lean et al. 2011).

Other than anomalies, NmF2 also exhibits solar cycle variation due to large thermospheric variations, primarily owing to the variation of the solar radiation. The NmF2 variations are observed to be linearly correlated with variation in solar flux during low solar activity due to lower thermospheric compression (Soloman et al. 2010). However, the ionospheric variations during the inclining and declining phases of the solar cycle show peculiar features (Bhuyan et al. 1983; Park et al. 2008).

The importance of TEC studies in the Indian Ocean region has tremendously increased because of the development of a new geo-economic region on the world map due to the busiest maritime route and airlink. As a result, accuracy of communication and navigation systems demands precise information about the dynamic ionosphere during different conditions which is also useful for the climate models. The ionospheric studies in the Indian Ocean region are limited due to the fewer IGS/ionosonde stations. Seasonal variations in TEC during low solar activity at Diego Garcia (Tsai et al. 2001), anomaly in the seasonal variations (Ouyang et al. 2008), effect of seasonal variations of TEC on morphology of EIA in the Indian-Australian sector (Zhao et al. 2009), hemispheric asymmetry of EIA (Xiong et al. 2013) have been reported. It is noted by literature survey that a very few studies on TEC variability were carried out in the Indian Ocean region (e.g., Kenpankho et al. 2011; Shreedevi et al. 2018 and references therein). However, these studies were performed using the IRI-2007/IRI-2012 model TEC data of a year or two years. As solar flux is the key input in IRI model, it becomes important to see the impact of the upgraded version IRI-2016 based on improved compositional model in the topside ionosphere and revised solar indices. This was the motivation to perform comparative analysis using the IRI-2016 model for a period encompassing different phases of the solar cycle.

Another model which is being used by ionospheric researchers to predict climatological picture of the ionospheric variability is the TIE-GCM (Perlongo et al. 2018; Rao et al. 2019b). In the present study, we have used IRI model as well as TIE-GCM to study TEC variability at the southern low latitude station COCO Island during the solar cycle 24. In our previous work (Rao et al. 2019b); we have mainly focused on the understanding of ionospheric anomalies at the northern low latitude station. In the present work, we have presented detailed statistical and regression analysis to understand TEC variability and comparative analysis of TEC trends for a complete solar cycle-24. Together with our previous work, this work gives an understanding of TEC variability and anomalies during the inclining, maximum, and declining phases of the solar cycle. Also, we have included different approaches to compare observed and modeled TEC trends. A huge data set used from GPS, IRI, and TIE-GCM provides an important and relevant aspect of TEC variability at southern low latitude. To the best of our knowledge, this work is the first of its kind wherein comparative analysis is done using different approaches for a complete solar cycle using three types of TEC data sets (One instrument and two models). Thus, the present study together with our previous study (Rao et al 2019b), would provide a complete picture of understanding the quiet time ionospheric climatology over northern and southern low latitudes.

2. Data set

The COCO Island (Geog. Lat. 12.20^{O} S; Geomag. Lat. 22.83^{O} S; Geog. Long. 96.80^{O} E) is an IGS station whose map of the geographic location is shown in Fig. 1. The Receiver Independent Exchange formatted TEC data were obtained through files transfer protocol using the link-ftp::://garner.ucsd.edu. The RINEX formatted TEC data were processed using Seemala's software tool namely

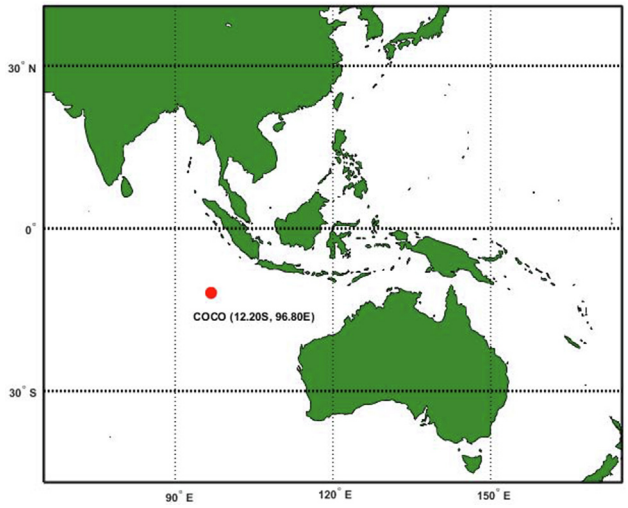

Fig. 1. Map showing the Geographic location of the COCO Island.

"GPS_Gopi_ver2.9.5" available at the web link- https://seemala.blogspot.com/2017/09/gps-tec-program-ver-295.html.The Seemala's software (Seemala and Valladares 2011) take care of calibration of the satellite (b_s) and receiver (b_R) errors (retrievable from: ftp://ftp.uni-be/aiub/CODE) inherent to the undifferenced pseudorange and carrier phase observations on L1 and L2 frequencies to obtain corrected slant total electron content (STEC). This software tool computes vertical total electron content (VTEC) using the following conversion formula given by Birch et al. (2002).

$$VTEC = (STEC - [b_R + b_S])/S(E_l) \quad (1)$$

The symbol $S(E_l)$ is a mapping function and it is computed as a reciprocal function of the cosine of the solar zenith angle (χ). χ depends on the satellite's elevation angle E_l in degrees at the ionospheric pierce point (IPP). It is further dependent upon mean Earth's radius R_E, ionospheric effective height h (h = 350 km) according to thin shell model, (Mannucci et al., 1953). In the rest of paper, the VTEC is referred as TEC.

$$S(E_l) = \frac{1}{\mathrm{Cos}(\chi)} = \left\{1 - \left(\frac{R_E \mathrm{Cos}(E_l)}{R_E + h}\right)^2\right\}^{-1/2} \quad (2)$$

We have used the model TEC data obtained from the empirical IRI-2016 model and the TIE-GCM of the Community Coordinated Modeling Center (CCMC) available at website: https://omniweb.gsfc.nasa.gov. We have modeled vertical TEC of IRI-2016 for a station COCO Island using standard IRI topside option NeQuick with URSI-88F top model through CCMC. The TIE-GCM model was first evolved by Roble et al. (1977), and it is consistently promoted by the National Center for Atmospheric Research (NCAR), USA. The advanced version is the TIE-GCM 2.0 (Soloman et al. 2016). The CCMC has provided the TIE-GCM TEC database for 2009–2017 under "Run on Request" mode. The monthly data files were published on the CCMC website at the link-https://ccmc.gsfc.nasa.gov. The data are available at the "view request result" interface with run registration number sardar_rao_xxxxxx_IT_y. Here × stands for the date on which the model runs and y is the run number. The 3D time series of data for a given location could be created at the web interface. The list of all the input parameters for both models are given in Table 1.

The F10.7 flux data are accessible from Space Physics Data Facility (SPDF) OmniWeb and the Ap index data is available at the World Wide Data center (WDC). The local time at COCO Island is given by LT = UT + 06:30 hrs.

3. Results and discussion

The period of this study encompasses the inclining phase (2009–2013), solar maximum (2013–2014), and declining phase (period 2015–2018) of solar cycle-24. It is depicted from the Fig. 2 that the level of F10.7 flux increases with the inclining phase of the solar cycle and becomes greater during the solar maximum and then decreases with the declining phase of the solar cycle. The Ap index's background level was almost steady (below 20 nT) throughout 2009–2018, indicating the less contribution of the geomagnetic activity in TEC variation during solar cycle-24. Fig. 2 also reveals that the TEC trend follows the variation of F10.7 flux during different phases of the solar cycle. However, space weather events like solar flares and geomagnetic storms also occurred during the period 2009–2018. Since the IRI/TIE-GCM model predicts the reliable data during geomagnetic quiet days only, the TEC data for the geomagnetically disturbed days when solar flares ≥ M3.4 class and Dst < -50 nT have been removed from the analysis. The ionospheric trends are closely dependent upon F10.7 flux trends (Laštovicka et al. 2006).

To look for the ionospheric trends, a linear regression analysis to determine the correlation between monthly mean values of F10.7 flux and TEC (see, Fig. 3) are carried out. Our analysis reveals a relatively high correlation (R) between the monthly mean GPS/model TEC values versus monthly mean F10.7 flux, (R = 0.77) for GPS-TEC, (R = 0.78) for IRI TEC, and R = 0.94 for TIE-GCM TEC. This implies that the F10.7 flux is the dominating agent to which the TEC variations could be attributed. Thus, a little contribution in TEC variation from other sources is also present that could not be determined by a linear fit. The difference in correlation coefficient for IRI and TIE-GCM with F10.7 flux is because of the seasonal biases of each model depending upon the chemistry involved in the development of the model.

Contour plots of hourly averaged monthly mean TEC values from GPS (left panel), IRI (middle panel) and TIE-GCM (right panel) are shown in Fig. 4 for the period 2009–2018. The Y ordinate of Fig. 4 gives the time in UT (4–16 UT). It can be seen from Fig. 4 that GPS-TEC and IRI-TEC maximize around 0600 UT ± 2 h (LT = UT +

0630 h) throughout 2009–2018. Leong et al. (2009) have reported that the diurnal maximum in TEC over Malaysia during the year 2008 occurs two hours after solar noon. It may be verified from the color scale that the variation of monthly mean TEC has a systematic pattern of increase and decrease with the solar cycle. During March-April and September-October for all the years, peaks in TEC show the notable semiannual oscillation in GPS TEC and model TEC. The semiannual variation is attributed to the change in column density ratio ΣO/N2 (Mendillo et al., 2005).

It can also be seen from the left panel of Fig. 4, that the strength of the second equinoctial peak in GPS TEC was larger than the first one during the period 2009–2013 and 2017–2018. During the period 2014–2016, the strength of the first peak was larger than the second one. Thus, an equinoctial asymmetry is present in TEC. Furthermore, IRI TEC also confers a similar equinoctial asymmetry (middle panel). Fig. 4 indicates greater GPS-TEC values in December (southern summer) than in June (southern winter) for 2009–2018. However, the solstice TEC difference becomes lesser with the inclining phase and increases with the declining phase of the solar cycle. This shows more December-June differences during low solar activity years and less difference during high solar activity years. It can be seen from the middle panel of Fig. 4 that the IRI model supports GPS-TEC variation during the solstices, wherein TEC was greater in December than in June for all the years during the solar cycle-24. The IRI 2016 model uses a topside ion composition model that provides the percentage of O+, H+, He+, and N + ions from the F2 peak up to 2000 km. Determination of electron density distribution at the F2 peak and above on a global scale can be an important contribution to the physical and empirical modeling of the ionosphere. Also, IRI model predictions are computed using ionosonde data and thus, the general feature of seasonal variation is assumed to be reflected in the IRI model.

The right panel of Fig. 4 shows the variation of monthly mean TEC obtained from the TIE-GCM. It is seen from Fig. 4 that the TIE-GCM TEC maximizes ~ 0800UT ± 2 h during the period 2009–2018. TIE-GCM TEC also shows the peaks during the March and September equinoxes of each year during the period 2009–2017. Thus, a semiannual anomaly is continuously present in TEC regardless of the level of solar activity. An equinoctial asymmetry can also be seen in the figure. However, it is not as systematic as seen from the IRI model and GPS TEC. Fig. 4 shows that the TIE GCM yields greater TEC values in December than in June for 2009–2014 and 2017. For the years 2015–2016, TEC values are observed to be slightly greater in June than in December. The results of Qian et al. (2009) also showed much weaker TIE-GCM seasonal amplitude of thermospheric density than the observations.

In our previous study (Rao et al. 2019b), we studied TEC variability at the northern low-latitude station Varanasi, India during the same period 2009–2018. Therefore here it would be interesting to look at similarities or differences of variability at both northern and southern low-latitude stations. It is observed that the nature of the appearance of double maxima during the solar cycle is consistent at both the northern and southern low-latitude stations. The IRI and TIE-GCM models also exhibit similar solar cycle variations at both the northern and southern latitude stations. However, the magnitude of model TEC values is observed to be more accurate over southern low latitudes. The R-value is computed ~ 0.82 between F10.7 flux & GPS TEC, 0.85 between F10.7 flux & IRI TEC, and 0.87 between F10.7 flux & TIE-GCM TEC at the northern low latitude station. The R-value is computed 0.78 between F10.7 flux & GPS/ IRI TEC and 0.94

Table 1
List of the input parameters used in IRI model and TIE-GCM is shown.

Input parameters for the IRI model and TIE-GCM	
IRI-2016	TIE-GCM
1. Daily F10.7	1. Daily F107
2. 81-day Running mean F10.7	2. 81-day center-averaged F10.7 solar index
3. 12-month running mean Sunspot number	3. Height limitation for Electron Content = 97–500 km.
4. 12-month running mean Ionosonde-based IG index,	4. Particle precipitation: Hemispheric Power in GW, obtained from 3-hour Kp index
5. Magnetic index (3-h ap, daily ap and 3-h_kp)	5. Ionospheric electric fields at high latitudes: Provided by Heelis model and Weimer model
6. Height limitation for Electron Content = 65–2000 km (Day time) and 80–2000 km (night time)	5(i). Inputs for Heelis model: Cross polar cap potential in kV, obtained from 3-hour Kp index Hemispheric Power in GW, obtained from 3-hour Kp index Optional (not implemented): y-component of the interplanetary magnetic field (By) in nT
7. Top side Electron density model-NeQuick	5(ii). Inputs for Weimer model: Interplanetary magnetic field, By and Bz, in nT Solar wind density and speed, ρ and v, in cm-3 and km s-1
8. Electron Density F peak model-URSI	
9. F peak height-AMTB2013	
10. Bottomside Thickness model-ABT-2009	
11. F1 occurrence probability- Scotto-1997 no L	
12. foF2 Storm model = on	6. Inputs for lower boundary: Diurnal and semi-diurnal migrating tides, specified by the Global Scale Wave Model
13. D region model-IRI-95	
14. Topside electron temperature-TBT2012 + SA	
15. Ion composition-RBV10/TBT15	
16. Auroral boundary = on	

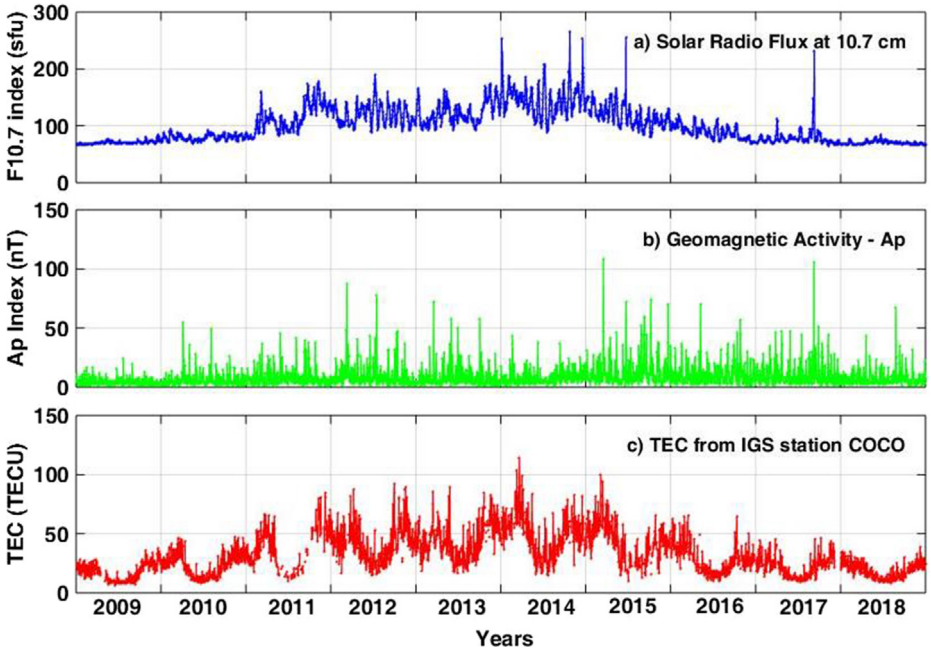

Fig. 2. Solar cycle variation of the F10.7 flux, Ap Index and GPS TEC during 2009–2018 is shown.

between F10.7 flux & TIE-GCM TEC at the southern low latitude station. The magnitudes of lowest and highest monthly mean TEC values is found to be higher at southern low latitude station compared to northern low latitude station. The presence of semiannual oscillation in TEC is found to be consistent during the solar cycle at two opposite hemispheric stations. Also, asymmetry in semiannual variation is observed in TEC over both stations. The presence of winter anomaly in the seasonal variation of TEC is not observed over the southern low latitude station throughout the solar cycle, whereas it is observed to be solar flux-dependent behaviour at the northern low latitude station. The detailing of solar flux-dependent characteristics of winter anomaly is explained and reported in some recent studies (e.g., Mikhailov and Perrone 2014; Yasyukevich et al. 2018; Rao et al. 2019b). At southern low latitudes, the winter anomaly is suppressed due to dominating presence of the annual component (Lee et al. 2011) due to the solstice difference of the Sun-Earth distance and the offset of the magnetic field in both hemispheres (Mallis and Essex 1993; Zeng et al. 2008; Liu et al. 2009). The observed seasonal variation in TEC at COCO Island is found to be consistent with Guo et al. (2015). In general, the seasonal trends in TEC obtained from GPS and models (IRI and TIE-GCM) are in agreement but a point-to-point deviation exists. In the following section 3.2, a comparative analysis between observed and modeled TEC is discussed.

3.1. Model TEC estimations and deviations

Fig. 4 shows the diurnal and seasonal pattern of monthly mean TEC of GPS and both the models. To understand the nature of deviations, the difference between the daily and seasonal TEC is computed by applying equation (3) at each hour of the day for a given month during the low solar activity year 2009 (Fig. 5) and high solar activity year 2014 (Fig. 6). The Positive difference in TEC (DTEC) shows level of underestimation and negative amplitude shows level of overestimation by the model.

$$DTEC = GPSTECvalue - ModelTECvalue_{(IRIorTIE-GCM)} \quad (3)$$

For showing the diurnal difference (Fig. 5) of observed and model TEC variation, the start day of a corresponding season for a given year is chosen when the Sun reaches the most southerly point in the sky during solstices and when the Sun passes over Earth's equator during equinoxes (refer Figs. 5.1–5.4 given in the supplementary material to see deviations in model TEC values on all days of the years 2009 and 2014). Fig. 5 reveals that the IRI model overestimates TEC values during morning and prenoon hours and underestimates during the noon hours for low solar activity year 2009 whereas, during the evening and night hours, almost no difference is observed. This result is consistent with the result of de Abreu et al. (2017) wherein they found better IRI-2012 modeled TEC estimations during night hours of low solar activity year 2009 at the southern EIA crest in the Brazilian sector. It is seen from the left panel of Fig. 5 that the extent of overestimations/ underestimations reached ± 10 TECU from morning to noon hours. The TIE-GCM TEC values are underestimated for all chosen days in low solar activity year 2009 except the noon hours on 22 September and during the post evening hours on 21 March. Also, the maximum underestimations are

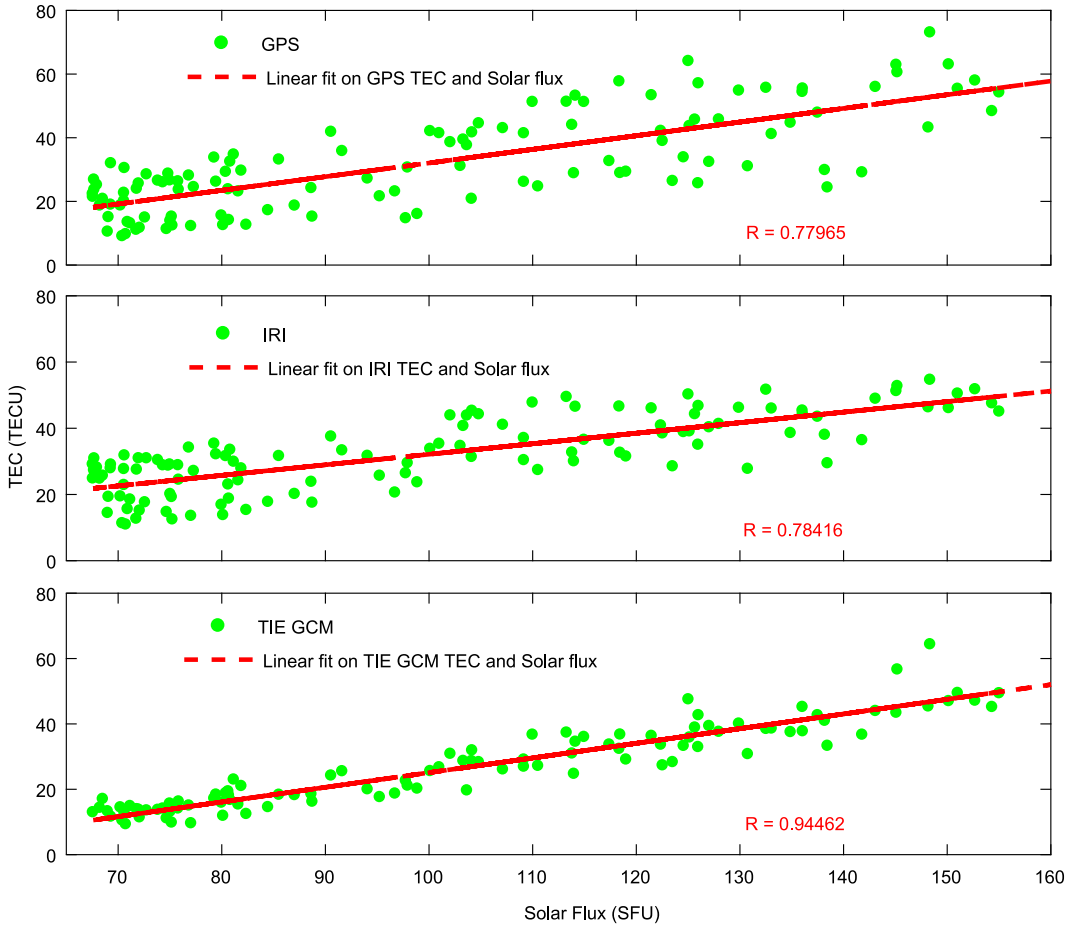

Fig. 3. Correlation curves between the F10.7 flux & GPS TEC (upper panel), IRI TEC (middle panel), and TIE GCM (lower panel) and is given.

observed on 21 December 2009. For the remaining days, the TIE-GCM model deviations are observed to be of the order of 5 TECU.

For a high solar activity year 2014, the difference between GPS and model(s) TEC is shown in the right panel of Fig. 5. Both the IRI and TIE-GCM model show a very high value (~55 TECU) of underestimation during 0500–1600 UT on 21 March 2014. On 22 June 2014, both models overestimated TEC except at 0900 UT. The overestimation level is four times greater for the IRI model from 0000 to 0800 UT. After that, both IRI and TIE-GCM overestimate TEC values with equal magnitude in decreasing order with the passage of the day. On 22 September 2014, the IRI model overestimated and the TIE-GCM model underestimated the TEC up to 0600 UT, and after that, both models overestimated TEC values up to 0900 UT. From 1000 UT onwards, both models estimated nearly the same value as that of the GPS values. On 21 December 2014, the IRI model underestimated TEC values during 0500–1100 UT and overestimates TEC values during the morning, post-noon, evening, and night hours. The TIE-GCM TEC values are found to be underestimated for the whole day except during 0900–1300 and 2200–2400 UT.

To examine the deviation in TEC values during seasons, we have computed the difference of seasonal trends of TEC derived from GPS and estimated from IRI and TIE-GCM models, and results are presented in Fig. 6. The seasonal values were computed by taking mean of respective months at each hour of the day (summer season: December-January, winter season: June-July, autumn equinox: March-April and vernal equinox: September-October). The IRI and TIE-GCM model deviations during the different seasons are shown by blue and yellow bars. Fig. 6 shows underestimation by the TIE-GCM model throughout the low solar activity year 2009. The underestimation level is as high as 10 TECU and as low as 2 TECU depending upon the local time (i.e. morning/noon/evening/night hours). Similar results of local time dependency of IRI-2012 modeled TEC estimations during different seasons at Port Blair and at Singapore in Indian Ocean region were reported by Chakraborty et al. (2014) and Kumar et al. (2014), respectively. The IRI TEC deviations are more significant for morning to noon hours and smaller for post noon, evening, and night hours throughout all the seasons. During the winter season, both IRI and TIE-GCM yield closer value to the observed values during the whole day.

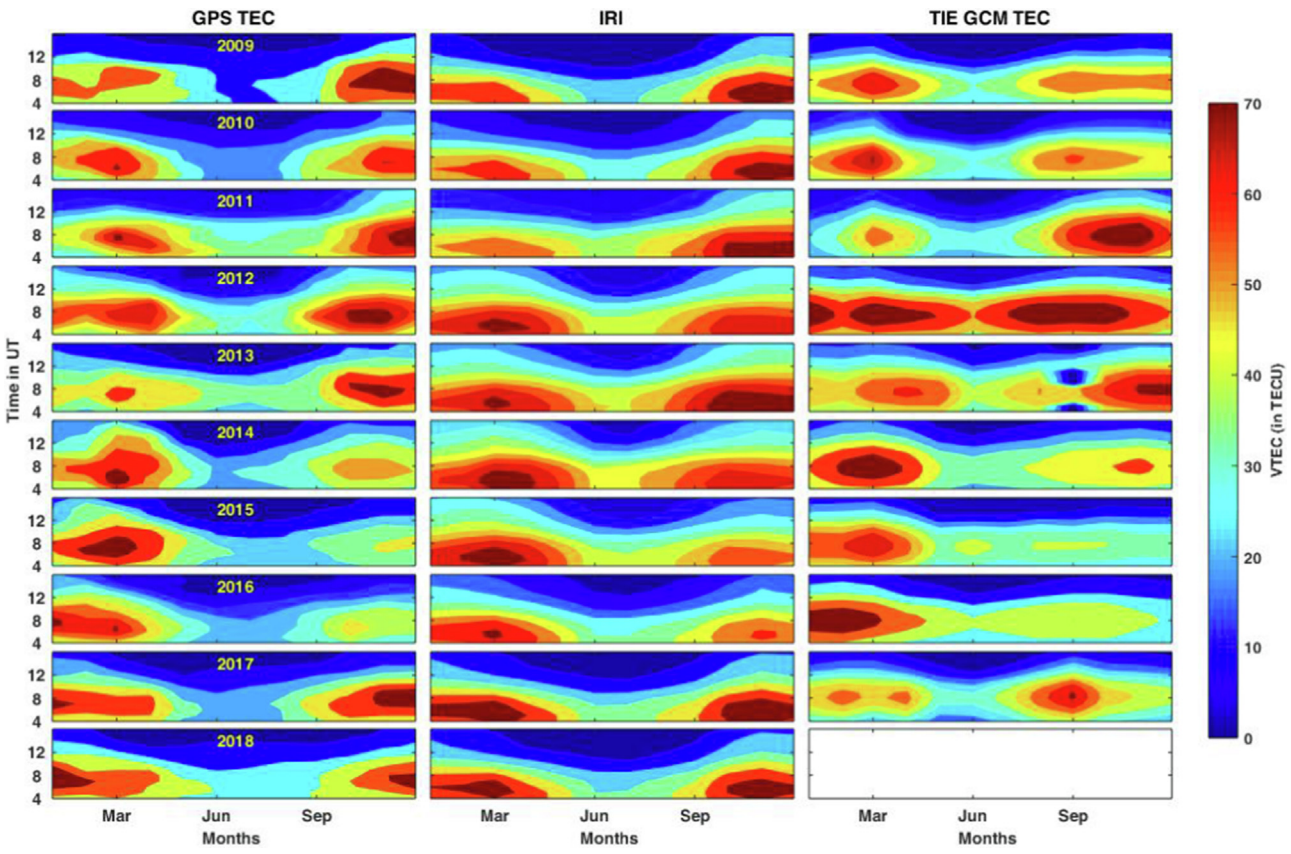

Fig. 4. Monthly mean variation of GPS-TEC (left panel) IRI-2016 TEC (middle panel) and TIE-GCM TEC (right panel) in time interval of 0400–1600 UT for the period 2009–2018 at COCO Island is presented.

Also, both models perform well during the night hours. It can be seen from the right panel of Fig. 6 that the IRI model underestimated TEC values by ~ 5 TECU during summer 2014 for all hours of the day, whereas overestimated during winter of 2014 for all hours of the day. However, overestimation is decreased from ~ 15 TECU in morning hours to ~ 2 TECU during late night hours. For autumn 2014, the IRI TEC values are greater during early morning hours and smaller during the rest of the day. Nearly the same trend is seen during the vernal equinox of 2014 wherein IRI values are higher during midnight to prenoon hours and smaller during noon to late evening hours. TIE-GCM overestimated the TEC values in winter 2014. It can be seen from the figure that the overestimation amplitude starts increasing from 0000 UT and became 15 TECU at ~ 1100 UT. Thereafter, level of overestimation decreases and became nearly equal to the magnitude of GPS TEC during night hours. In summer 2014, TIE-GCM also overestimated TEC values except during the period 0800–1200 UT, where it underestimated TEC values by ~ 10 TECU. During the vernal and autumnal equinoxes, the TIE-GCM model underestimated during the 0000–1600 UT. The correlation coefficients and root mean square error (RMSE) between the GPS and model values (IRI/TIE-GCM) from Figs. 5 and 6 are shown in Table 2.

Table 2 shows an excellent correlation (greater than 0.80) for both IRI and TIE-GCM models during the low and high solar activity year. RMSE of the IRI and GPS-TEC shows a good performance on selected days of the low solar activity year 2009. For the high solar activity year case (i.e., the year 2014), the IRI model's performance is found to be poor. A value of 37 RMSE on 21 March 2014 for the IRI model reveals high value of deviation in the equinox of high solar activity year. Earlier, Venkatesh el al. (2014) also reported that the IRI-2012 model performance decreases during the inclining phase of solar cycle in the Brazilian sector and greater deviations of model TEC during the equinoctial and summer months. RMSE of the TIE-GCM TEC from the GPS-TEC shows comparatively good performance on the chosen days of low and high solar activity year except for a few cases. For example, the RMSE for 22 December 2009 and 21 March 2014 is computed to be ~ 10.52 TECU and 31.21 TECU, respectively. Thus, IRI and TIE-GCM performance shows highly deviated value on 21 March 2014.

As depicted in Fig. 6, there is a significant similarity in seasonal trends between the GPS TEC and IRI model predictions. The seasonal deviation of model TEC has also been tested by correlation coefficient and RMSE computation (Table 2). The correlation coefficient of IRI versus

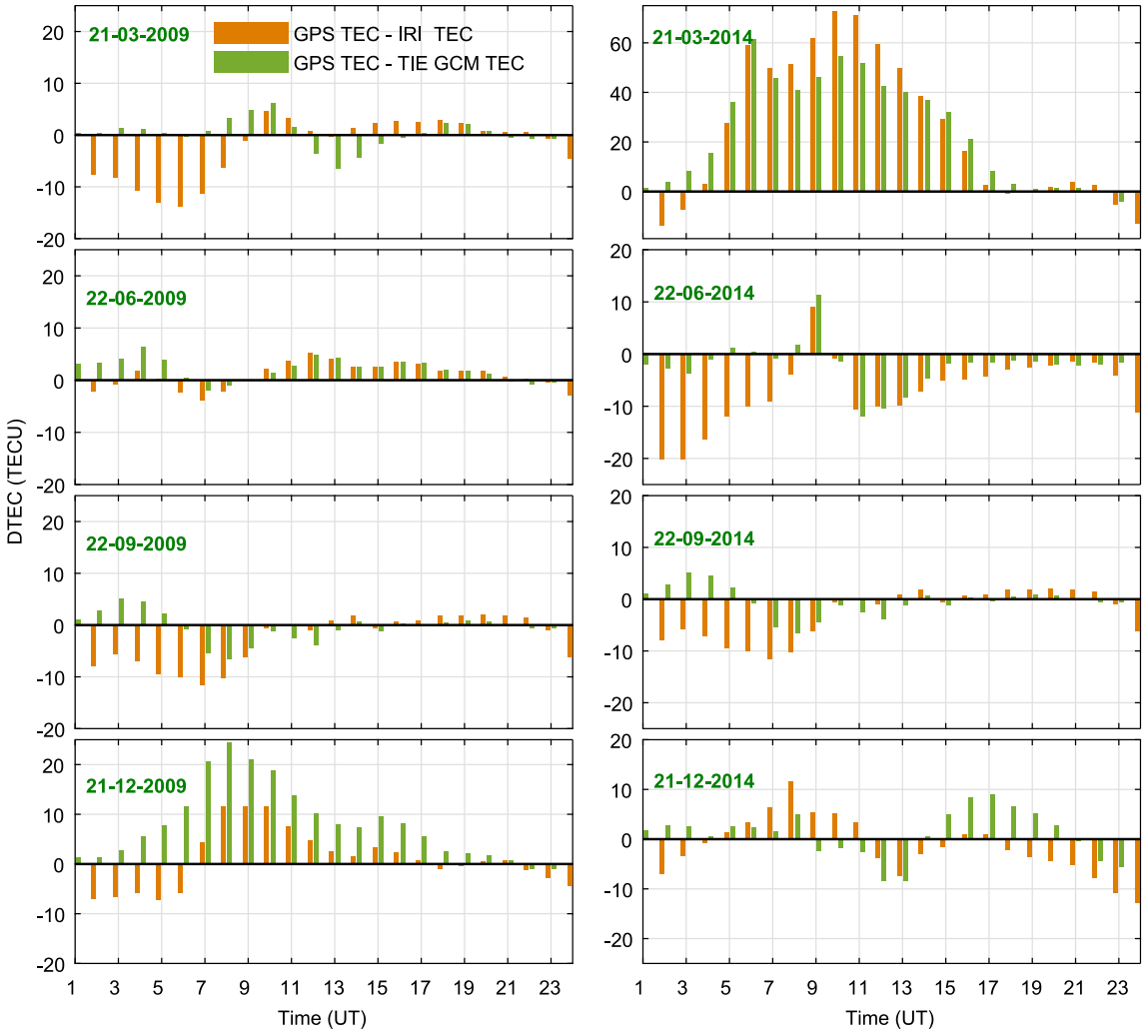

Fig. 5. A deviation of diurnal pattern of TEC on a start day of a corresponding season for a low solar activity year 2009 (left panel) and high solar activity year 2014 (right panel) is presented. The underestimation and overestimation is shown by Positive and negative amplitudes.

GPS TEC is found to be greater than 0.80 for low and high solar activity years during all seasons and it is found to be greater than 0.90 in the summer and autumn of the low solar activity and the summer and winter of high solar activity year 2014. In TIE-GCM, the model estimations are highly correlated with GPS TEC values with an average R greater than 0.95. Table 2 also shows the difference between the GPS TEC values and the IRI/TIE-GCM predictions by RMSE. By examining the RMSE values shown in Table 2 corresponding to seasons for the model and GPS TEC, it is seen that the IRI and TIE-GCM model performed better during different seasons of low solar activity year. The precision of TIE-GCM in terms of RMSE during the summer and autumn of high solar activity year 2014 is found to be relatively better. Additionally, the quantitative assessment of models have been studied using equations (4) & (5) (Ikubanni et al. 2014) and equation (6) (Oyeyemi et al. 2013).

$$\text{Mean Difference}\,(MD) = \frac{1}{n}\sum_{i=1}^{n}(X_{obs} - X_{model}) \tag{4}$$

Root Mean Square Error $(RMSE)$

$$= \sqrt{\frac{1}{n}\sum_{i=1}^{n}(X_{obs} - X_{model})^2} \tag{5}$$

Relative Deviation Module Mean, $(RDMM)$

$$= \frac{1}{n}\sum_{i=1}^{n}\frac{|X_{obs} - X_{model}|}{X_{obs}} \tag{6}$$

Here n is the number of data points and X_{obs} and X_{model} are the observed and predicted values (IRI/TIE-GCM), respectively.

The results employing above equations are shown in Fig. 7. Here it is important to mention that we have shown only the fitting curves (refer supplementary Figs. 7.1–7.3 to see the background variations of MD, RDMM and RMSE values). The abscissa of Fig. 7 shows days of a given year and also classified in terms of seasons. The dates of equinoxes and solstices are chosen to mark the beginning and end seasons in a year. The Blue and red curves in Fig. 7 shows the respective polynomial fit for IRI and TIE-GCM, respectively. The pink curve shown in supplemen-

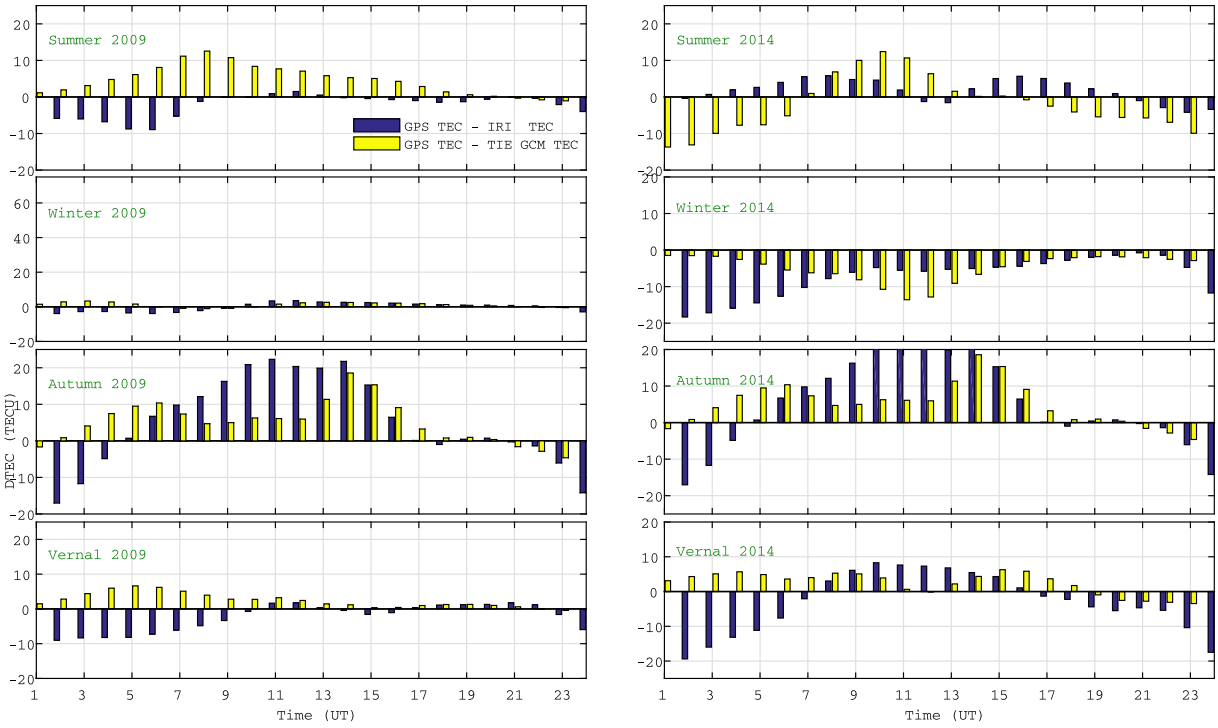

Fig. 6. A deviation of seasonal pattern of TEC for a low solar activity year 2009 (left panel) and high solar activity year 2014 (right panel) is presented. A level of underestimated and overestimated model TEC values is shown by positive and negative amplitudes.

tary Figs. 7.1–7.3 is for the IRI model, and the green curve is shown for TIE-GCM. The MD values for the IRI model during 2009–2010 and 2016–2018 are found to be smaller than those in high solar activity years. Thus, the IRI model performance is observed to be better during low solar activity years. Another noteworthy point is that both models manifested minimal deviation in autumn and winter, especially during the low solar activity years. For the low solar activity years 2009–2010, MD values for IRI are negative (overestimations), whereas MD values for TIE-GCM are positive (underestimations) during all seasons.

For the years 2011–2013, the polynomial fit curve shows the sinusoidal behaviour wherein the degree of overestimation/underestimations periodically changes with the change of seasons. Most of the TIE-GCM MD values in summer, autumn, and vernal seasons of the years 2011–2013 are positive, which means the TIE-GCM model gives an underestimation of the TEC. The IRI MD values for the summer season of 2011–2013 show negative values showing overestimations. For the autumn, IRI MD values are positive for 2011, whereas it becomes negative for 2012–2013. The level of RDMM is appeared to be binned within the limit of 1 TECU. The RDMM values for IRI model do not show any seasonal dependency during all the years of low solar activity. However, a slight variation in IRI RDMM values is seen during equinoxes of high and moderate solar activity. For the high solar activity year 2014, both IRI and TIE GCM RDMM values showed larger values during post autumn to mid of winter. Thus, a good correlation between GPS TEC and models is observed during low solar activity and deviations are seen during high and moderate activity period.

The RMSE values of both models are found to be smaller and more stable during the winter throughout the period 2009–2018. Significant variations in RMSE values are seen during summer and vernal months during moderate and high solar activity. RMSE variations are found to be deviated more for TIE-GCM compared to IRI values. In general, MD, RMDD and RMSE analysis show good agreement of both the models with GPS TEC, particularly during low solar activity years. Seasonal biases in TEC values are also noted during different years.

It is clear from the value of the correlation coefficient (R) shown in Fig. 8 that certain linear correlations exist between the GPS and IRI TEC. IRI model predictions correlate well with GPS TEC values during 2009–2010, years of low solar activity year. The coefficient of determination is computed to be of 81 % during the year 2009 and 65 % during the year 2010. For the remaining years, the value of the coefficient of determination is computed to be of ~ 45–50 %. Thus the regression determines a good correlation between GPS and IRI values during the 24th solar minimum when the level of F10.7 flux was almost constant for the period 2008–2010. Since the F10.7 flux is the key input parameter in the IRI simulation, a less correlation during the ascending and descending phase of solar activity might be due to the solar hysteresis (Rao et al. 2019b). In contrast, the TIE-GCM TEC values are not alike with

Table 2
The correlation coefficients and RMSE values between the IRI/TIE-GCM and the GPS hourly (Fig. 5) and seasonal (Fig. 6) TEC values are shown.

Solar Activity level	Dates(DD-MM-YYYY) /Seasons	IGS and IRI TEC		IGS and TIE GCM TEC	
		Correlation Coefficient 'R'	RMSE	Correlation Coefficient 'R'	RMSE
Hourly TEC values corresponding to Fig. 5					
Low Solar Activity Year	21–03-2009	0.83949	6.1048	0.91985	2.6567
	22–06-2009	0.81999	2.5600	0.76429	2.8800
	23–09-2009	0.87266	5.5962	0.83895	2.7447
	22–12-2009	0.87648	5.7634	0.95394	10.5200
High Solar Activity Year	21–03-2014	0.83790	37.0100	0.98011	31.2100
	22–06-2014	0.84437	10.0200	0.92943	4.7500
	23–09-2014	0.89902	12.2300	0.97901	9.5800
	22–12-2014	0.97158	6.0673	0.96316	4.6748
Seasonal TEC values corresponding to Fig. 6					
Low Solar Activity Year 2009	Winter	0.86454	2.5775	0.89102	1.7298
	Summer	0.93537	3.8618	0.98039	5.8994
	Autumn	0.90251	4.7602	0.96956	3.1010
	Vernal	0.8158	5.4455	0.98496	2.5857
High Solar Activity Year 2014	Winter	0.93285	9.3413	0.96099	6.0265
	Summer	0.91112	7.8782	0.98744	3.4829
	Autumn	0.85827	9.6239	0.98836	3.8834
	Vernal	0.86674	12.9541	0.97804	7.5065

the observations. The values of the correlation coefficient between GPS and TIE-GCM are found to be less than 0.50 during most of the years. This shows a weak positive correlation between GPS and TIE-GCM TEC values. The coefficient of determination is found to be of $\sim$ 20 % for low and moderate solar activity years and $\sim$ 42 % for high solar activity year 2014. The variation determined by the regression line is very small which shows distinct chemistry involved in the TIE-GCM model. It is seen from Fig. 8 that the scattered data points were concentrated at the head side of the regression line during the year 2009–2010 and 2017–2018 because of low solar activity. The scattered points extended along the regression line for the inclining or declining solar activity years. This shows relatively small TEC values during low solar activity years.

It is noted from the above results that the IRI and TIE-GCM models are capable to reproduce the gross feature of local time, diurnal, semiannual, seasonal, and solar cycle variations in TEC but, a one-to-one mapping is not observed between modeled and GPS TEC values. In general, the statistical analysis reveals that the mapping between modeled and observed values is surjective during low solar activity years and injective during high solar activity years. IRI model deviations are primarily due to the inadequate input data set from the Indian Ocean region. For the given times and regions where there are few or no data sources, IRI's predictive capability may be relatively low (Bilitza et al. 2014). Using the GPS, IRI-2007, and IRI-2012 TEC data over Thailand in the Indian Ocean region, Chowdhary et al. (2015) have concluded that the difference in TEC deviation in the range of 5–15 TECU at night and noon hours is related to the difference of slab thickness in the ionosphere between the IRI model and the measured data. In equinoxes and summer months, the TIE-GCM TEC is observed to underestimate usually during noontime. For the winter months of high solar activity years, TIE-GCM overestimates the TEC. In the winter months of low solar activity, TIE-GCM TEC is underestimated by $\sim$ 2 TECU. For low and high solar activity years, models TEC are seen to be overestimated at mid and post-midnight hours. The present analysis estimates as low as 2 TECU and as high as 20 TECU deviations of IRI/TIE-GCM TEC compared to GPS-TEC.

The differences between GPS TEC and model-derived values may also arise due to the location of COCO Island in the equatorial electrodynamic zone which is affected by the EEJ and neutral winds that are not taken care of in the model simulation. Deviations of the TIE- GCM estimations from GPS TEC observations are related to chemistry and neutral winds. Thermospheric neutral density and composition exhibit a strong seasonal variation, with maxima near the equinoxes, and a minimum during the summer. The seasonal variation in the ratio of atomic oxygen to molecular nitrogen (O/N2) has been considered as a cause of similar variation in the peak electron density of the F2 layer (Rishbeth et al. 2000). The TIE-GCM model evolves upper atmospheric chemistry, and electrodynamics self consistently. It does produce annual/semiannual variations in thermospheric parameters. Since TEC is mostly weighted around the F2 layer, a higher O/N2 ratio leads to more TEC through increased photoelectron production and/or decreased charge exchange involving N2. Neutral winds can also enhance or reduce the TEC by pushing ions up or down along magnetic field lines to altitudes with different recombination rates. The higher wind speed had the potential for the stronger driving of ions up and down field lines, resulting in larger and smaller TEC values. However, the TIE-GCM model rarely includes winds faster than 200 m/s and almost nil above 350 m/s (Perlongo et al. 2018).

The deviation in the magnitude of TEC values is also attributed to the ionosphereic height assumed in simula-

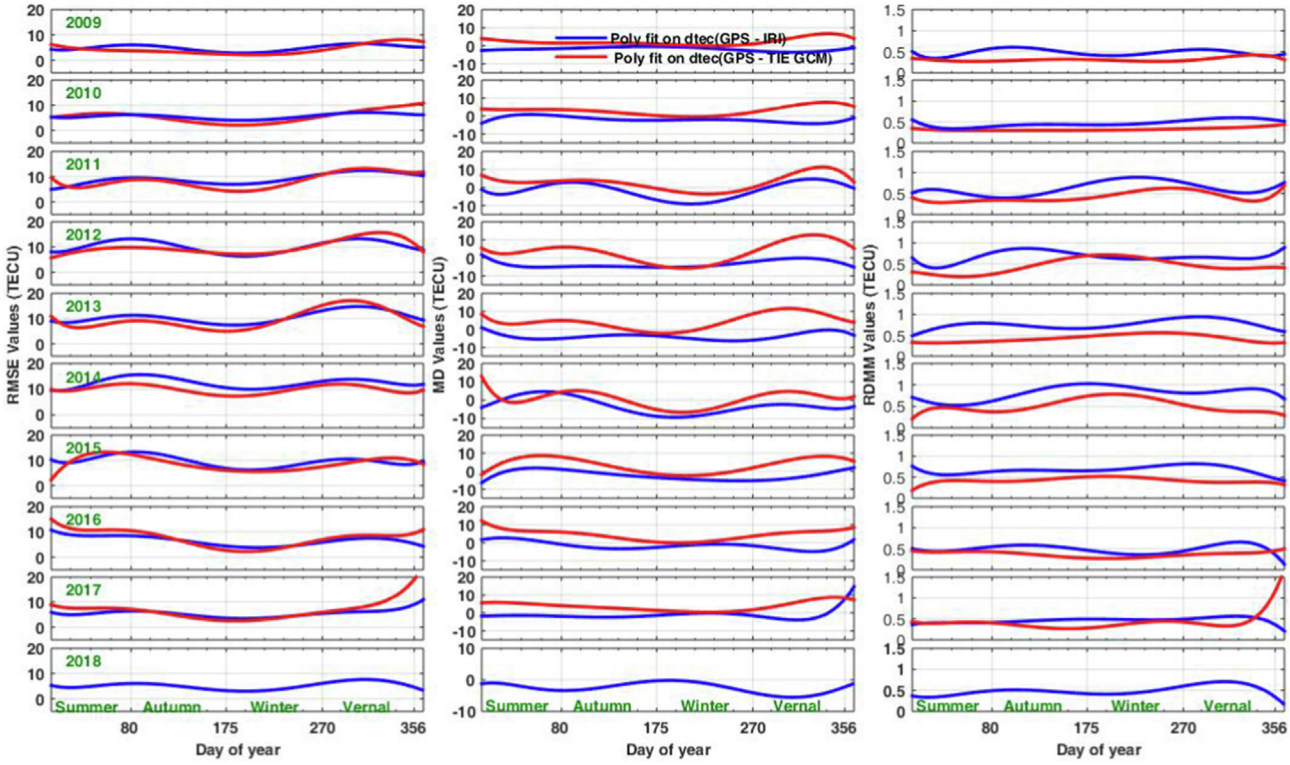

Fig. 7. The 9th order polynomial fits for IRI (blue) and TIE-GCM (red) obtained from RMSE (left panel), MD (middle panel) and RDMM (right panel) values between GPS – IRI TEC and GPS - TIE GCM TEC for the period 2009–2018 at COCO Island is presented.

tion. TIE-GCM extends to 500–800 km altitude and does not include the He^{+} that dominate the plasmosphere above 1000 km. However, plasmospheric contribution is low but extends out to approximately the orbital height of GPS satellites (Elizabeth et al. 2011). Shim et al. (2017) reported plasmospheric contribution in the global averaged TEC of the order of 4 TECU that corresponds to about 10–20 % depending upon the phase of solar activity. Comparatively better TEC estimations by the IRI model is probably due to the additional height limit of up to 2000 km. However, there is an added 10∼20 % TEC exceeding the 2000 km altitude (Makela et al. 2000).

4. Summary

The present study gives comparative results on TEC variations at a southern low latitude station COCO Island using GPS TEC and two climate models (IRI model, and TIE-GCM). Statistical and regression analyses are used and results are discussed in terms of different factors affecting the performance of models. The results of this study are also significant as the variations and trends in TEC are tested using the dataset of almost complete solar cycle covering different phases of solar cycle. The main results are summarised in the following.

1. IRI and TIE-GCM models are found to be capable of replicating the trends and pattern of TEC variations. However, both model's values show local time and seasonal biases. It is observed that the GPS and IRI TEC show peak around 0600 UT ± 2 h, whereas TIE-GCM TEC peak is ∼ 0800 UT ± 2 h.
2. IRI and TIE-GCM diurnal TEC estimations are found to be comparable with the GPS TEC during night hours throughout the solar cycle. IRI TEC estimations during day hours of low solar activity year are observed to be underestimated and overestimated by ± 10 TECU whereas TIE-GCM TEC values are observed to be mostly underestimated during low solar activity years by ± 5 TECU.
3. For the high solar activity year, the deviations observed from both models lie between 5 and 10 TECU depending upon local time except on 21 March 2014, when the IRI and TIE-GCM model TEC showed exceptionally high (∼55 TECU) underestimated value.
4. RMSE analysis for diurnal TEC profile of IRI model shows good performance during low solar activity year and relatively poor performance during high solar activity year. The same analysis for TIE-GCM model showed good performances during low as well as high solar activity year. The correlation analysis supported an excellent (correlation coefficient >0-80) capability of both models in predicting diurnal variation of TEC profile.
5. In the case of seasonal variation, TIE-GCM model underestimated (between 2 and 10 TECU) during low solar activity year. The same for the IRI model during low solar activity year are found to depend upon local

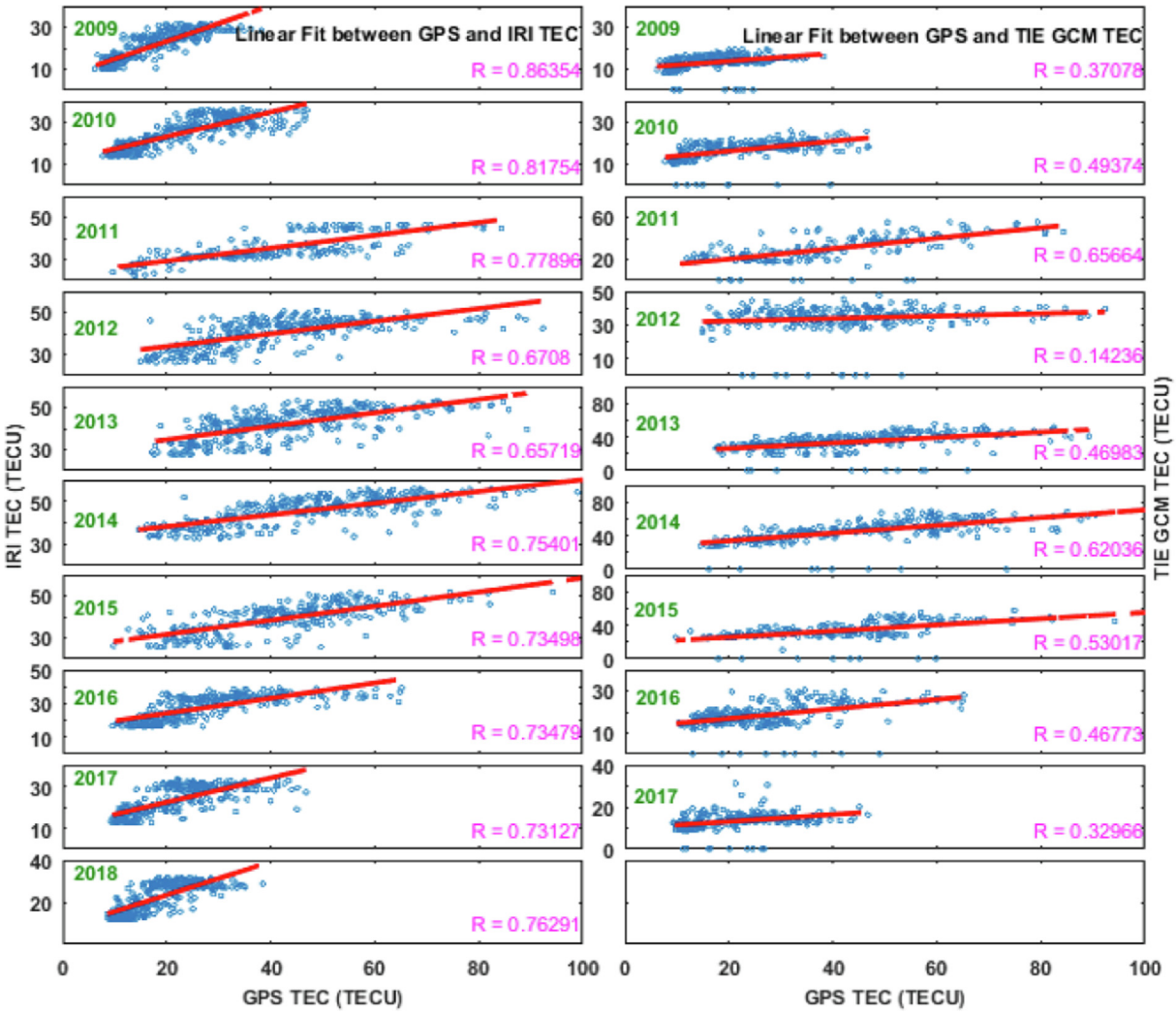

Fig. 8. Comparison of the GPS TEC values and models (IRI and TIE-GCM) TEC values at the COCO Island for the period 2009–2018 using linear fitting is shown.

time and deviations are computed from −10 TECU to + 20 TECU. The least deviated TEC values are simulated by both models for the winter season of low solar activity year.

6. The seasonal IRI and TIE-GCM TEC deviations during high solar activity period are computed with amplitude of ∼ ±2 TECU to ± 15 TECU depending upon local time and seasons. The GPS versus model seasonal TEC correlation coefficient shows a high (greater than 0.95 for TIE-GCM, and 0.90 for IRI) value. RMSE analysis of seasonal TEC variation during low solar activity year shows better precision for IRI and TIE-GCM model.
7. A statistical approach using MD, RMSE, and RDMM methods show surjective and injective mapping between model and observed TEC values during low solar activity and high solar activity periods respectively. These approaches reveal local time, seasonal and solar activity dependency of model precision that could be applied to obtain bijective mapping between modeled and observed TEC values.
8. A regression analysis shows that the IRI and TIE-GCM model are correlated linearly during low solar activity but the linearity breaks during ascending and descending phase of the solar cycle due to the hysteresis effects in the solar cycle. Thus the predictions show homoscedasticity during low solar activity year and heteroscedasticity during high and moderate solar activity year.

This work shows that despite reproducing the typical climatology of the ionosphere, both models have significant divergences in terms of point-to-point matching of TEC profile. Following may be the likely reasons for deviations; (i) GPS TEC data coverage at ocean sector, (ii) electric field, neutral wind and compositional model and (ii) height limitation of simulation. So, the present study draws attention towards adopting the above factors for improvements

in the IRI and the TIE GCM model so that these climate models can be used with more reliability in the real time operational forecasting.

Declaration of Competing Interest

The authors declare that they have no known competing financial interests or personal relationships that could have appeared to influence the work reported in this paper.

Acknowledgments

Council of Scientific and Industrial Research (CSIR), New Delhi sponsors this work under Scientist's Pool Scheme awarded to Senior Research Associate Dr. S S Rao (File No. 13(9203-A)/2021- POOL Dated 28/12/2021). Author A.K Singh is thankful to SERB, New Delhi for CRG project (file No: CRG/2019/000573). The authors are thankful to the Community Coordinated Modeling Center, NASA, for providing TIE-GCM data. Authors are thankful to the Prof. R.P. Singh (Retired Professor from BHU Varanasi, India) for valuable editing in the manuscript.

Appendix A. Supplementary material

Supplementary data to this article can be found online at https://doi.org/10.1016/j.asr.2022.12.030.

References

Balan, N., Otsuka, Y., Fukao, S., Abdu, M.A., Bailey, G.J., 2000. Annual variations of the ionosphere: A review based on MU radar observations. Adv. Space Res. 25 (1), 153–162. https://doi.org/10.1016/S0273-1177(99)00913-8.

Bhuyan, P.K., Tyagi, T.R., Singh, L., Somayajulu, Y.V., 1983. Ionospheric electron content measurements at a northern low mid latitude station through half a solar cycle. Indian J. of Radio Space Phys. 12, 84–93 http://nopr.niscpr.res.in/handle/123456789/36746.

Bilitza, D., Altadill, D., Zhang, Y., Mertens, C., Truhlik, V., Richards, P., Reinisch, B., 2014. The International Reference Ionosphere 2012-a model of international collaboration. J. Space Weather Space Clim. 4 (A07), 12. https://doi.org/10.1051/swsc/2014004.

Birch, M.J., Hargreaves, J.K., Bailey, G.J., 2002. On the use of an effective ionospheric height in electron content measurement by GPS reception. Radio Sci. 37, 1–19 https://doi:10.1029/2000RS00260.

Chakraborty, M., Kumar, S., Kumar, B.D., Guha, A., 2014. Latitudinal characteristics of GPS derived ionospheric TEC: a comparative study with IRI 2012 model. Ann. Geophys. 57 (5), A0539. https://doi.org/10.4401/ag-6717.

Chapman, S., 1931. The absorption and dissociative or ionizing effect of monochromatic radiation in an atmosphere on a rotating earth. Proc. Phys. Soc. (London) 43 (1), 26–45 http://doi:10.1088/0959-5309/43/1/305.

Chen, Y., Liu, L., Le, H., Wan, W., Zhang, H., 2016. Equatorial ionization anomaly in the low-latitude topside ionosphere: Local time evolution and longitudinal difference. J. Geophys. Res. Space Physics 121 (7), 7166–7182. https://doi.org/10.1002/2016JA022394.

Chowdhary, V.R., Tripathi, N., Arunpold, S., Durairaju, K.R., 2015. Characterization of GPS-TEC in a low-latitude region over Thailand during 2010–2012. Ann. Geophys. 58 (5), A0533. https://doi.org/10.4401/ag-6717.

de Abreu, A.J., Martin, I.M., de Jesus, R., Bolzan, M.J.A., Venkatesh, K., Fagundes, P.R., Alves, M.A., Gende, M., Kumar, S., 2017. Comparison of GPS-TEC measurements with IRI2012-TEC predictions in the Brazilian sector during the unusual solar minimum 2009. Ann. Geophys. 60, 0331. https://doi.org/10.4401/ag-7300.

Duncan, R.A., 1969. F-region seasonal and magnetic-storm behaviour. J. Atmos. Terr. Phys. 31 (1), 59–70. https://doi.org/10.1016/0021-9169(69)90081-6.

Elizabeth, P., Manuel, P., Spalla, P., Philip, M., Matt, K., 2011. A Review of Higher Order Ionospheric Refraction Effects on Dual Frequency GPS. Surv. Geophys. 32, 197–253. https://doi.org/10.1007/s10712-010-9105-z.

Guo, J., Li, W., Liu, X., Kong, Q., Zhao, C., Guo, B., 2015. Temporal Spatial Variation of Global GPS Derived Total Electron Content. 1999–2013. PLoS ONE 10(7). https://doi.org/10.1371/journal.pone.0133378.

Ikubanni, S.O., Adeniyi, J.O., Obrou, O.K., 2014. Monthly mean foF2 model for an African low-latitude station and comparison with IRI. Adv. Space Res. 53 (4), 635–646. https://doi.org/10.1016/j.asr.2013.12.016.

Kendall, P.C., 1964. On the equations governing diffusion in the F_2-layer. J. Atmos. Terr. Phys. 26 (5), 624–626. https://doi.org/10.1016/0021-9169(64)90194-1.

Kenpankho, P., Supnithi, P., Sugawa, T., Maruyamaet, T., 2011. Variation of ionospheric slab thickness observations at Chumphon equatorial magnetic location. Earth Planet Sp. 63, 359–364. https://doi.org/10.5047/eps.2011.03.003.

Kumar, S., Leong T.E., Razul, S. G., Samson See C. M., Singh, D., 2014. Validation of the IRI-2012 model with GPS-based ground observation over a low-latitude Singapore station. Earth Planet Sp. 66, 17. https://doi.org/10.1186/1880-5981-66-17.

Laštovicka, J., Mikhailov, A.V., Ulich, T., Bremer, J., Elias, A.G., Ortiz˘ de Adler, N., Jara, V., Abarca del Rio, R., Foppian, A.J., Ovalle, E., Danilov, A.D., 2006. Long-term trends in foF2: a comparison of various methods. J. Atmos. Terr. Phys. 68(17), 1854–1870. https://doi.org/10.1016/j.jastp.2006.02.009.

Lean, J.L., Meier, R.R., Picone, J.M., Emmert, J.T., 2011. Ionospheric total electron content: Global and hemispheric climatology. J. Geophys. Res. 116, A10318. https://doi.org/10.1029/2011JA016567.

Lee, W.K., Kil, H., Kwak, Y.S., Wu, Q., Cho, S., Park, J.U., 2011. The winter anomaly in the middle-latitude F region during the solar minimum period observed by the Constellation Observing System for Meteorology, Ionosphere, and Climate. J. Geophys. Res. 116 (A2), A02302. https://doi.org/10.1029/2010JA015815.

Leong, S.K., Musa, T.A., Abdullah, K., Othman, R., Lim, S., Rizos, C., 2009. GPS-derived local TEC mapping over peninsula Malaysia during solar minimum of sunspot cycle 24. Conference: Proceedings of South East Asian Survey Congress. Bakosurtanal. http://handle.unsw.edu.au/1959.4/unsworks_55643.

Liu, L.B., Wan, W.X., Ning, B.Q., Zhang, M.L., 2009. Climatology of the mean TEC derived from GPS global ionospheric maps. J. Geophys. Res. 114 (A06), 308. https://doi.org/10.1029/2009JA014244.

Ma, R., Xu, J., Liao, H., 2003. The features and a possible mechanism of semi-annual variation in the peak electron density of the low latitude F_2 layer. J. Atmos. Solar-Terr. Phys. 65 (1), 47–57. https://doi.org/10.1016/S1364-6826(02)00192-X.

Makela, J.J., Sixto, A., Gonzalez, S.A., MacPherson, B., Pi, X., Kelley, M.C., Sultan, P.J., 2000. Intercomparisons of total electron content measurements using the Arecibo incoherent scatter radar and GPS. Geophysical Research Letters 27 (18), 2841–2844. https://doi.org/10.1029/2000GL000023.

Mallis, M., Essex, E.A., 1993. Diurnal and seasonal variability of the southern-hemisphere main ionospheric trough from differential phase measurements. J. Atmos. Solar-Terr. Phys. 55 (7), 1021–1037. https://doi.org/10.1016/0021-9169(93)90095-G.

Mannucci, A.J., Wilson, B.D., Edwards, C.D., 1993. A new method for monitoring the Earth's ionospheric total electron content using the

GPS global network. paper presented at ION GPS-93, Inst. of Navigation, 1323–1332. http://hdl.handle.net/2014/36277.

Martyn, D.F., 1953. Electric currents in the ionosphere. III. Ionization drifts due to winds and electric fields. A 246 (913), 306–320. https://doi.org/10.1098/rsta.1953.0018, Philos. Trans. R. Soc. London. Ser..

Mayr, H.G., Mahajan, K.K., 1971. Seasonal variation in the F_2 region. J. Geophys. Res. 76 (4), 1017–1027. https://doi.org/10.1029/JA076i004p01017.

Mendillo, M., Huang, C.L., Pi, X., Rishbeth, H., Meier, R., 2005. The global ionospheric asymmetry in total electron content. J Atm Solar-Terr Phys. 67 (15), 1377–1387. https://doi.org/10.1016/j.jastp.2005.06.021.

Mikhailov, A.V., and Perrone L., 2014. Comment on "The winter anomaly in the middle-latitude F region during the solar minimum period observed by the Constellation Observing System for Meteorology, Ionosphere, and Climate" by W. K. Lee, H. Kil, Y.-S. Kwak, Q. Wu, S. Cho, and J. U. Park. J Geophys Res (Space Phys), 119, 7972–7978. https://doi.org/ 10.1002/2014JA020185.

Millward, G.H., Moffett, R.J., Quegan, S., Fuller-Rowell, T.J., 1996. Ionospheric F_2 layer seasonal and semi-annual variations. J. Geophys. Res. 101 (A3), 5149–5156. https://doi.org/10.1029/95JA03343.

Ouyang, G., Jian, W., Jinling, W., David, C., 2008. Analysis on Temporal-Spatial Variations of Australian TEC. Observing our Changing Earth International Association of Geodesy Symposia. https://doi. https://doi.org/10.1007/978-3-540-85426-5_86.

Oyeyemi, E.O., Adewale, A.O., Adeloye, A.B., Olugbon, B., 2013. An evaluation of the IRI-storm time model at low latitude stations. Adv. Space Res. 52 (10), 1737–1747 http://www.dx.doi.org/10.1016/j.asr.2013.04.027.

Pacheco, E.E., Yizengaw, E., 2013. The day-to-day longitudinal variability of the global ionospheric density distribution at low latitudes during low solar activity. J. Geophys. Res. 118 (4), 1813–1823. https://doi.org/10.1002/jgra.50241.

Park, S.M., Kim, H., Min, S., Park, J., Lee, J.H., Kil, H., Paxton, L.J., Su, S.-Y., Lee, J., Min, K.W., 2008. Effects of solar activity variations on the low latitude topside nighttime ionosphere. Adv. Space Res. 42 (4), 626–633. https://doi.org/10.1016/j.asr.2007.11.031.

Perlongo, N.J., Ridley, A.J., Cnossen, I., Wu, C., 2018. A year-long comparison of GPS-TEC and global ionosphere-thermosphere models. J. Geophys. Res. Space Phys. 123, 1410–1428 (2018). https://doi.org/10.1002/2017JA024411.

Pulido, A.M., Garat, E.F., 1997. The ionospheric F2 region winter anomaly and its dependence on solar activity in the northern and southern hemispheres. Geophysica International. ISSN, 0016–7169.

Qian, L., Solomon, S.C., Kane, T.J., 2009. Seasonal variation of thermospheric density and composition. J. Geophys. Res. 114 (A01312) https://doi:10.1029/2008JA013643.

Rao, S.S., Sharma, S., Pandey, R., 2019a. Study of solar flux dependency of the winter anomaly in GPS TEC. GPS Solution 23, 4. https://doi.org/10.1007/s10291-018-0795-x.

Rao, S.S., Chakraborty, M., Sanjay, K., Singh, A.K., 2019b. Low latitude ionospheric response from GPS, IRI and TIE-GCM TEC to Solar Cycle 24. Astrophysics and Space Science 364, 216. https://doi.org/10.1007/s10509-019-3701-2.

Rishbeth, H., 1998. How the thermospheric circulation affects the ionospheric F_2-layer. J. Atmos. Sol. Terr. Phys. 60 (14), 1385–1402. https://doi.org/10.1016/S1364-6826(98)00062-5.

Rishbeth, H., Müller-Wodarg, I.C.F., Zou, L., Fuller-Rowell, T.J., Millward, G.H., Moffett, R.J., Idenden, D.W., Aylward, A.D., 2000. Annual and semiannual variations in the ionospheric F2-layer. II: Physical discussion. Ann. Geophys. 18, 945–956. https://doi.org/10.1007/s00585-000-0945-6.

Rishbeth, H., Muller-Wodarg, I.C.F., 2006. Why is there more ionospheric in January than in July? The annual asymmetry in the F_2-layer. Ann. Geophys. 24, 3293–3311. https://doi.org/10.5194/angeo-24-3293-2006.

Rishbeth, H., Setty, C.S.G.K., 1961. The F-layer at sunrise. J. Atmos. Sol. Terr. Phys. 21, 263–276 https://doi:10.1016/0021-9169(61)90205-7.

Roble, R.G., Dickinson, R.E., Ridley, E.C., 1977. Seasonal and solar-cycle variations of zonal mean circulation in the thermosphere. J. Geophys. Res. 82 (35), 5493–5504. https://doi.org/10.1029/JA082i035p05493.

Seemala, G.K., Valladares, C.E., 2011. Statistics of total electron content depletions observedover the South American continent for the year 2008. Radio Science 46, RS5019. https://doi.org/10.1029/2011RS004722.

Shim, J.S., Jee, G., Scherliess, L., 2017. Climatology of plasmaspheric total electron content obtained from Jason 1 satellite. J. Geophys. Res. Space Physics 122, 1611–1623. https://doi.org/10.1002/2016JA023444.

Shreedevi, P.R., Choudhary, R.K., Yadav, S., Thampi, S.V., Ajesh, A., 2018. Variation of the TEC at a dip equatorial station, Trivandrum and a mid-latitude station, Hanle during the descending phase of the solar cycle 24 (2014–2016). J. Atmos. Sol. Terr. Phys. 179, 425–434. https://doi.org/10.1016/j.jastp.2018.09.010.

Solomon, S.C., Woods, T.N., Didkovsky, L.V., Emmert, J.T., Qian, L., 2010. Anomalously low solar extreme-ultraviolet irradiance and thermospheric density during solar minimum. Geophys. Res. Lett. 37 (16), L16103. https://doi.org/10.1029/2010GL044468.

Tsai, H.F., Liu, J.Y., Tsai, W.H., Liu, C.H., Tseng, C.L., Wu, C.C., 2001. Seasonal variations of the ionospheric total electron content in Asian equatorial anomaly regions. J. Geophys. Res. 106 (A12), 30363–30369. https://doi.org/10.1029/2001JA001107.

Venkatesh, K., Fagundes, P.R., de Seemala, G.K., Jesus, R., de Abreu, A. J., Pillat, V.G., 2014. On the performance of the IRI-2012 and NeQuick2 models during the increasing phase of the unusual 24th solar cycle in the Brazilian equatorial and low-latitude sectors. J. Geophys. Res. Space Physics 119, 5087–5105. https://doi.org/10.1002/2014JA019960.

Wang, G.J., Shi, J.K., Wang, Z., Wang, X., Romanova, E., Ratovsky, K., Polekh, N.M., 2017. Solar cycle variation of ionospheric parameters over the low latitude station Hainan, China, during 2002–2012 and its comparison with IRI-2012 mode. Advances in Space Research 60 (2017), 381–395. https://doi.org/10.1016/j.asr.2016.12.013.

Xiong, C., Lühr, H., Ma, S.Y., 2013. The magnitude and inter-hemispheric asymmetry of equatorial ionization anomaly-based on CHAMP and GRACE observations. J. Atmos. Sol. Terr. Phys. 105–106, 160–169. https://doi.org/10.1016/j.jastp.2013.09.010.

Yasyukevich, Y.V., Yasyukevich, A.S., Ratovsky, K.G., Klimenko, M.V., Klimenko, V.V., Chirik, N.V., 2018. Winter anomaly in NmF2 and TEC: when and where it can occur. J. Space Weather Space Clim. 8, A45. https://doi.org/10.1051/swsc/2018036.

Zeng, Z., Burns, A., Wang, W., Lei, J., Soloman, S., Syndergaard, S., Qian, L., Kuo, Y.H., 2008. Ionospheric annual asymmetry observed by the COSMIC Radio Occultation measurements and simulated by the TIE-GCM. J. Geophys. Res. 113, A07305. https://doi.org/10.1029/2007JA012897.

Zhao, B., Wan, W., Liu, L., Ren, Z., 2009. Characteristics of the ionospheric total electron content of the equatorial ionization anomaly in the Asian-Australian region during 1996–2004. Ann. Geophys. 27, 3861–3873. https://doi.org/10.5194/angeo-27-3861-2009.

Zou, L., Rishbeth, H., Müller-Wodarg, I.C.F., Aylward, A.D., Millward, G.H., Fuller-Rowell, T.J., Idenden, D.W., Moffet, R.J., 2000. Annual and semiannual variations in the ionosphere F_2-layer I. Model. Ann. Geophys. 18, 927–944. https://doi.org/10.1007/s00585-000-0927-8.